Hindawi
Laser and Particle Beams
Volume 2022, Article ID 3049749, 9 pages
https://doi.org/10.1155/2022/3049749

CAMBRIDGE
UNIVERSITY PRESS

Research Article

Plasma Spectroscopy on Hydrogen-Carbon-Oxygen Foam Targets Driven by Laser-Generated Hohlraum Radiation

Bubo Ma,[1] **Jieru Ren**,[1] **Shaoyi Wang**,[2] **Xing Wang**,[1] **Shuai Yin**,[1] **Jianhua Feng**,[1] **Wenqing Wei**,[1] **Xing Xu**,[1] **Benzheng Chen**,[1] **Shisheng Zhang**,[1] **Zhongfeng Xu**,[1] **Zhongmin Hu**,[1] **Fangfang Li**,[1] **Hao Xu**,[1] **Taotao Li**,[1] **Yutian Li**,[1] **Yingying Wang**,[1] **Lirong Liu**,[1] **Wei Liu**,[1,3] **Quanping Fan**,[2] **Yong Chen**,[2] **Zhigang Deng**,[2] **Wei Qi**,[2] **Bo Cui**,[2] **Weimin Zhou**,[2] **Zongqing Zhao**,[2] **Zhurong Cao**,[2] **Yuqiu Gu**,[2] **Leifeng Cao**,[4] **Rui Cheng**,[5] **Quanxi Xue**,[6] **Dieter H. H. Hoffmann**,[1] **and Yongtao Zhao**[1]

[1]*MOE Key Laboratory for Nonequilibrium Synthesis and Modulation of Condensed Matter, School of Physics, Xi'an Jiaotong University, Xi'an 710049, China*
[2]*Science and Technology on Plasma Physics Laboratory, Laser Fusion Research Center, China Academy of Engineering Physics, Mianyang 621900, China*
[3]*Xi'an Technological University, Xi'an 710021, China*
[4]*Advanced Materials Testing Technology Research Center, Shenzhen University of Technology, Shenzhen 518118, China*
[5]*Institute of Modern Physics, Chinese Academy of Sciences, Lanzhou 730070, China*
[6]*State Key Laboratory of Laser Interaction with Matter, Northwest Institute of Nuclear Technology, Xi'an 710049, China*

Correspondence should be addressed to Yongtao Zhao; zhaoyongtao@xjtu.edu.cn

Received 9 February 2022; Revised 26 May 2022; Accepted 31 May 2022; Published 17 June 2022

Academic Editor: Dimitri Batani

The laboratory generation and diagnosis of uniform near-critical-density (NCD) plasmas play critical roles in various studies and applications, such as fusion science, high energy density physics, astrophysics as well as relativistic electron beam generation. Here we successfully generated the quasistatic NCD plasma sample by heating a low-density tri-cellulose acetate (TCA) foam with the high-power-laser-driven hohlraum radiation. The temperature of the hohlraum is determined to be 20 eV by analyzing the spectra obtained with the transmission grating spectrometer. The single-order diffraction grating was employed to eliminate the high-order disturbance. The temperature of the heated foam is determined to be $T = 16.8 \pm 1.1$ eV by analyzing the high-resolution spectra obtained with a flat-field grating spectrometer. The electron density of the heated foam is about $N_e = 4.0 \pm 0.3 \times 10^{20}\text{cm}^{-3}$ under the reasonable assumption of constant mass density.

1. Introduction

Research into the matter under extreme conditions represents a frontier of experimental and theoretical techniques and requires infrastructure at the most technologically advanced level. Currently, a number of laser and particle beam facilities are operating, or are under construction and nearing completion. The most prominent example presently is the National Ignition Facility (NIF, Livermore, California), where next to stockpile stewardship issues, the physics of inertial confinement fusion is addressed [1]. In Europe, a network of laser facilities providing infrastructure for extreme light is operational [2]. In China, the laser fusion center in Mianyang is an example that in this context we want to refer to [3]. The highest level of energy concentration in space and time is currently achieved with laser light. In many standard approaches to high energy density physics experiments, low entropy laser radiation is transformed into high entropy thermal radiation, and the experimental method that we present here uses just this method. A power

reactor for fusion energy requires a high-efficiency driver. For experiments to study basic physics phenomena of high energy density, the driver efficiency is of less, or of no concern. Lasers, like the one used at the National Ignition Facility, do not meet the efficiency requirements for inertial fusion energy. They start with 422 MJ stored in capacitor banks to produce less than 2 MJ of Fusion power. Therefore, particle beams to induce high energy density in the matter should not be ignored [4, 5], since the efficiency to convert electric power into kinetic energy of an ion may well be over 20% [6, 7]. Laser and particle beams, as well as pulsed power devices, are important tools to generate matter under extreme conditions. Here we discuss a method that is particularly suited to produce conditions, as they prevail in stellar atmospheres and allow high-resolution spectroscopy as well as the measurement of transport properties and energy loss of ions in this environment.

Most experiments dealing with laser-plasma interaction and associated plasma phenomena use direct laser irradiation of the target (see recent examples [8–11]). In these experiments, steep gradients in pressure, density, and temperature and strong time dependence are unavoidable and reduce the precision of the obtained data, and require detailed simulation analysis. Laser speckles, which are caused by the coherent nature of laser light propagating through the glass surfaces of the laser system, are an additional source of inhomogeneous target irradiation. This effect can be mitigated by two-sided irradiation of the target foil, and it was applied to increase the precision of energy loss measurements in experiments at GSI-Darmstadt [12, 13], where two laser systems PHELIX [14] and nhelix [15] are available. In these experiments, the experimental data and two-dimensional simulation of the free electron density demonstrated that the nonuniformities were strongly reduced. However, in this case, plasma properties can only be analyzed by spectroscopic methods up to the critical density of the applied diagnostic laser. The warm dense matter part of the target is still terra incognita and must be addressed by simulation.

An alternative method is to use low-density foam targets in open geometry or encapsulated in a millimeter size hohlraum, which is heated by thermal radiation generated in an attached hohlraum. This method was pioneered at GSI-Darmstadt by Rosmej et al. and is documented in many publications [16–18]. Since in this laboratory there is a long tradition to investigate the stopping power of ionized matter for heavy ions, the available wealth of energy loss data can in turn be used to deduce plasma density and plasma properties with ns resolution [19–22]. In summary, the technique to indirectly heat foam targets with broadband thermal radiation is well established. Besides, high precision experiments require to have as much uniformity as possible. The method we describe here is characterized by superior properties with respect to target uniformity, scale length, negligible electromagnetic field effect, and lifetime [16–18, 23], as compared with the direct laser heating method [8–11, 24, 25]. The prize to pay is the lower plasma temperature that can be achieved. For the experiments we had in mind [23, 26], it was however just the right regime.

2. Description of the Experiment

The experiment was carried out at the XG-III laser facility of the Laser Fusion Research Center in Mianyang [27]. The envisioned experiments required a homogeneous plasma with well-characterized parameters. Therefore, we decided to heat a foam CHO target by laser-generated hohlraum radiation in the soft X-ray regime, to take advantage of the aforementioned properties [16–18]. In our setup (see Figure 1), the foam target is attached to the open lower end of the hohlraum.

According to previous experiments, there is a time window of about 15 ns (from 5 ns to 20 ns after the onset of the laser pulse). Within this period, the target temperature is rising without substantial expansion of the bulk material. The voids of the foam sample are filled by the expanding material and in good approximation, the line density stays constant. Therefore, the target may be considered quasi-static. As an improvement to previous work, we also diagnosed the hohlraum conditions with a single-order diffraction grating spectrometer [28], to exclude the influence of high-order diffraction.

In Figure 1, we present an outline of the irradiation scheme and the target coupling to the hohlraum. A cylinder made from steel constitutes the hohlraum with ~1 mm in diameter and ~1.8 mm in height. The inner hohlraum wall was gold-coated since high Z material ensures a high diffusive resistivity of the inner wall for thermal X-rays. The open entrance hole for heating ns laser is situated at a height of ~1.2 mm with a diameter of ~0.6 mm. Depending on the laser parameters, the efficient conversion of laser light into hohlraum thermal soft X-rays in the temperature regime between 10 and 100 eV can be achieved [17], and from the previous results [16], the conversion efficiency of laser energy into hohlraum X-rays reaches 17%.

The foam target consists of tri-cellulose acetate (TCA, $C_9H_{16}O_8$). It is a very low-density material with a mass density of $\rho = 2\text{mg/cm}^3$ and a total thickness of 1 mm. It is attached to the lower end of the hohlraum cylinder and mounted to a stainless-steel holder. This sample was selected since its composition promised to reproduce the atmospheric conditions of a peculiar white dwarf (H1504 + 65 see [26]) when turned into a plasma. Moreover, the hydrodynamic time scale for expansion is slow and thus favorable for experiments. Simulation results indicate a hydro-response time in the ns regime and the foam starts to expand visibly about 20 ns after the onset of the laser pulse. Due to the large penetration depth of soft X-rays, quasi-isochoric heating is achieved. Once heated by soft X-rays from hohlraum radiation, the material expansion occurs inside the target between the sponge-like structures, and this micro expansion leads to target homogenization. The unique property of a foam target with respect to its temporal evolution is mainly due to the supersonic propagation character of the generated radiation heat wave. Thus, the plasma stays at its initial average density during the heating process, and the radiation energy transfer is much faster than the thermal expansion of the plasma [16–18]. The simulation [17] shows that the foam layer becomes homogeneous and the temperature reaches

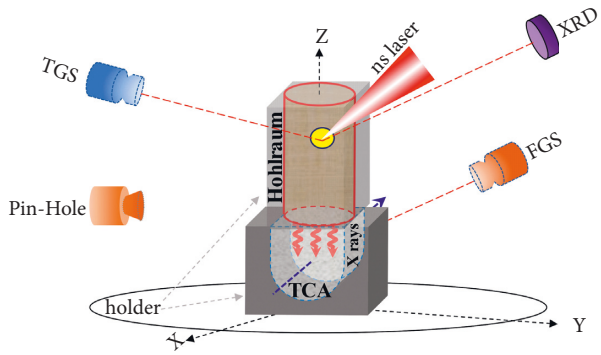

FIGURE 1: Geometry of the setup. The target consists of TCA foam attached to the lower side of the cylindrical Au-hohlraum. The foam and the hohlraum were supported by a stainless-steel holder. There are two free surfaces perpendicular to the blue-dashed arrow for diagnostics. The flat-field grating spectrometer (FGS) was obliquely positioned toward the backside of the foam target to measure the plasma radiation. Thus, the hohlraum radiation was effectively shielded. The X-ray diode (XRD), as well as the transmission grating spectrometer (TGS), with a single-order diffraction grating was directed toward the laser entrance hole to measure the hohlraum radiation. The pinhole (PH) camera was aimed at about 50° relative to the X-axis to image the expansion of hohlraum and foam plasma emitted from the laser entrance hole and the free surface of the foam target in the direction of X axis, respectively.

the maximum at about 3–4 ns after the start of the ns laser irradiation. Later, at 10–25 ns, the foam remains at a rather flat density and temperature distribution.

We used an ns laser pulse of 2 ns with a total pulse energy of 150 J. The beam was focused onto the open entrance hole under 45° to irradiate the wall of the gold converter. The generated soft X-ray flux subsequently irradiated and heated the foam target to the plasma state with the characteristic properties of being homogeneous, long-lived, large scale, and quasistatic. The plasma diagnostic equipment includes different tools to measure the radiative characteristics of the hohlraum and foam target. The transmission grating spectrometer (TGS), outfitted with a single-order diffraction grating (1000 lines per mm) and a slit of 100 μm, is coupled to a charge-coupled device (CCD) for the measurement of the gold hohlraum radiation. This has the advantage of significantly filtering the high-order components with moderate diffraction efficiency both in the visible light and soft X-ray regions, as well as the extreme ultraviolet regions [29]. The high-resolution flat-field grating spectrometer (FGS), with a grating of 1200 lines per mm, coupled to an image plate (BAS-IP TR 2025 of FUJI IMAGING PLATE) was used to record the emission spectra of CHO plasma. A detailed analysis of the image plate sensitivity is given in ref [30], and the response was taken into account in the reconstruction of the emission spectra. The X-ray diode (XRD) with Au cathode covering Ti filter was used for the time-resolved measurement of the soft X-ray flux generated in the Au-hohlraum below 400 eV with a temporal resolution of 100 ps, and the pinhole camera (PH) was used to characterize the gold hohlraum plasma and the resulting plasma.

3. Results and Discussion

3.1. Plasma Generation and Measurement of Radiative Properties. Since the heating process of the foam sample is determined by the properties of the soft X-ray flux from the hohlraum converter, the characterization of the hohlraum X-ray radiation is a necessary first step, the result is shown in Figure 2(a). The duration and amplitude of the soft X-ray signal indicate that the effective heating time of the X-rays is about 6 ns for the 2 ns/150 J laser pulse. The pinhole camera shown in the experimental setup of Figure 1 was fitted with a calibrated Fuji image plate and served to take an X-ray image of both the ionized foam plasma and the hohlraum radiation. Since the pinholes are not covered by any filters and all photons within the response range of the image plate are collected. The pinhole images are presented in Figure 2(b).

The X-ray spectrum (see Figure 3, red line) emitted from the hohlraum was measured with a transmission grating spectrometer (TGS) coupled with a single-order diffraction grating to effectively exclude the influence of high-order diffraction. The blue line in Figure 3 is a black body radiation fit to the X-ray spectrum corresponding to a radiation temperature of 20 eV. The deviation from the black body radiation spectrum is mainly due to contributions from the radiation from the gold hohlraum.

3.2. The Plasma Diagnostic. Figure 4 shows the high-resolution emission spectrum emitted from the foam target turned into plasma. In general, the energy of free electrons is described by a distribution. In the ideal case of thermal equilibrium, it is a Maxwell–Boltzmann distribution. Therefore, a continuous spectrum is emitted, originating from "free-bound" and "free-free" transitions, constituting the Bremsstrahlung background. Electronic transitions between ionic or atomic energy levels, so-called "bound-bound" transitions, are the origin of isolated ionic or atomic emission lines. The measured spectrum, therefore, is a superposition of isolated emission lines and a continuous background and contains a wealth of physical information due to the complex atomic processes and structures of plasma [31, 32].

The resonant lines of helium-like carbon ions (4.025 nm, 1s-2p) dominate the short-wavelength part of the spectrum, while at the long-wavelength position, Beryllium-like (62.973 nm, 2s-2p) and Boron-like (55.450 nm, 2s-2p) oxygen ions emerge. Some well-resolved and high-intensity characteristic lines in the middle-wavelength range were selected as wavelength references, such as 15.032 nm (OVI 2s-3p), 17.320 nm (O VI 2p-3d), and 19.253 nm (O V 2p-3d), which were also selected in previous projects for spectral lines identification [33–35]. According to the wavelength and intensity data provided by the National Institute of Standards and Technology (NIST) database [36], the experimental lines, both well-resolved and some blended lines, were well-identified for the ion species and charge states. In our experiments, the spectral lines were mainly attributed to the transitions of 2s-np, 2p-ns, 2p-np, and 2p-nd ($n = 2$–6) for O III-VI and C IV-V ions, which are induced by L-shell ionization processes of carbon and oxygen. This indicates

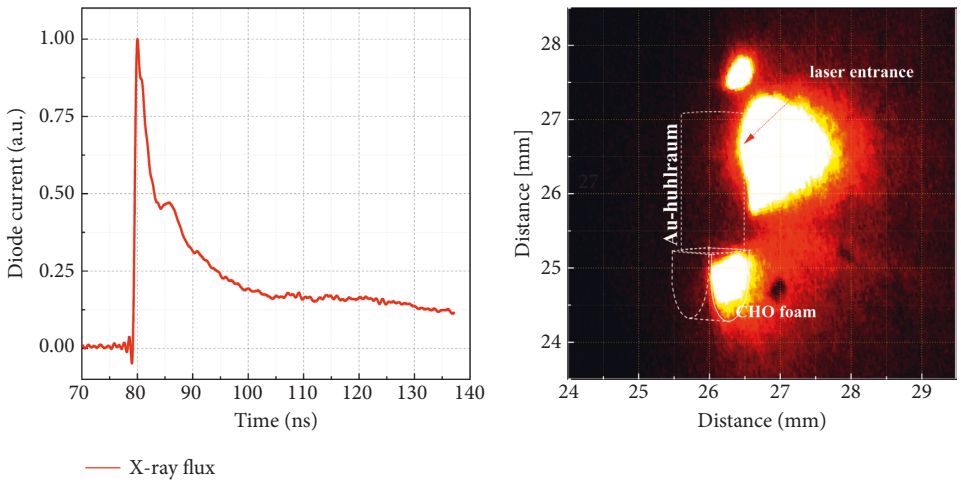

FIGURE 2: (a) The duration of the converter radiation pulse recorded by the X-ray diode is 5–7 ns; (b) the image of the pinhole camera with the outer features of the target geometry from the side at an angle of about 50° with respect to the *X*-axis.

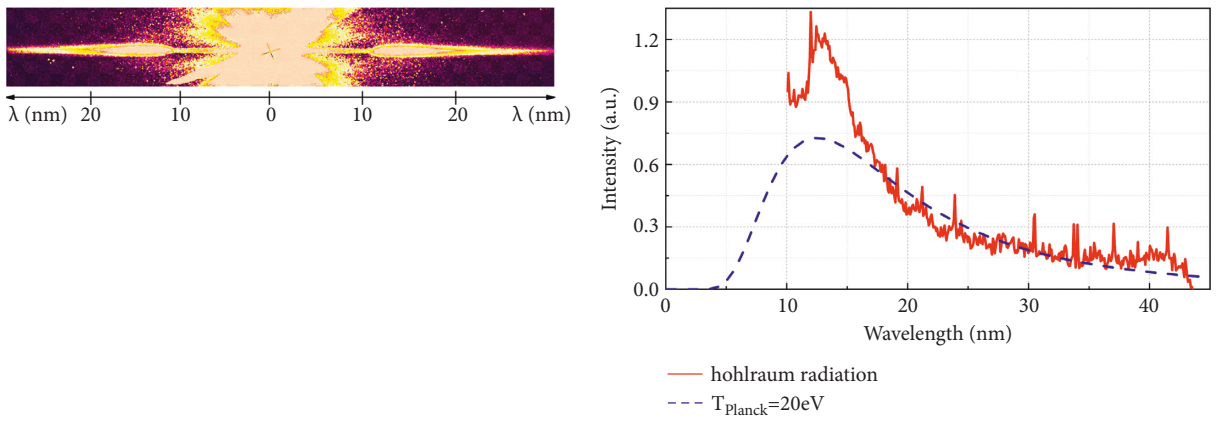

FIGURE 3: Measured spectrum of the gold hohlraum. (a) Raw spectra of the hohlraum radiation recorded by TGS and (b) the reconstructed spectral distribution of the 20-eV black body radiation curve.

that the free plasma electrons originate mainly from the ionization processes of valence electrons.

The flat-field grating spectrometer was calibrated with the Hefei Synchrotron Radiation Light Source [37, 38]. The wavelength accuracy is about 0.003 nm [39]. The wavelength resolution depends on the photon energy E, and we achieved $E/\Delta E \sim 300$ at $E = 62$ eV or equivalently at a photon wavelength of 20 nm. There is an intensity uncertainty of about 11% according to the calibration of the sensitivity curve for the Typhoon FLA 7000 imaging plate scanner. This includes 10% uncertainties due to experimental conditions, such as the instability of the light source and scanner system, the spatial roughness of the imaging plate, and 5% uncertainties for the calculation of electron numbers [40, 41].

The relative intensity of emission lines with the same lower level is very sensitive to the electron temperature T_e and density n_e. Therefore, the intensity ratio of characteristic lines is a useful tool for diagnosing the plasma parameters. Assuming that the conditions for Boltzmann distribution of the upper levels are met, the radiation intensity I_{mn} when an electron transits from energy level m to level n, can be expressed as: $I_{mn} = NA_m h\nu \exp(-\Delta E_{mn}/kT_{ex})$, where N, g_m, A_m $h\nu$, ΔE_{mn}, and k, are the total number of atoms, statistical weight, transition probability, photon energy, excited level energy, and the Boltzmann constant, respectively. T_{ex} is the excitation temperature. This shows the obvious dependence on the temperature T_{ex} and the weak dependence on electron density. When the conditions of local thermodynamic equilibrium (LTE) are fulfilled (the excitation temperature is equal to the electron temperature), the relative emission intensity and excitation temperature satisfies [42]:

$$\ln \frac{I_{mn}\lambda_{mn}}{A_m g_m} = -\frac{E_m}{kT_{ex}} + \ln \frac{N(T)}{U(T)}, \quad (1)$$

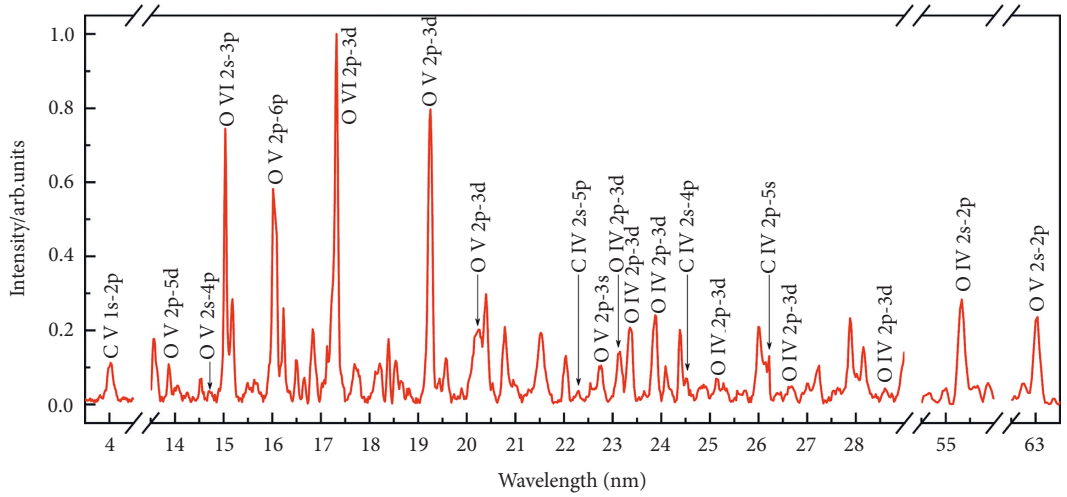

FIGURE 4: Plasma emission spectra are dominated by oxygen lines. Here the continuous radiation background is already subtracted. The intensity was normalized at the maximum value, and the main lines were denoted by wavelength and transition.

where $U(T)$ is the partition function and λ_{mn} is the transition wavelength.

This equation indicates that $\ln(I_{mn}\lambda_{mn}/A_m g_m)$ is proportional to the upper level energy E_m for the same atom or ion lines, and the slope is $-1/kT_{ex}$, which contains the temperature information of the plasma. Therefore, the temperature can be obtained without detailed knowledge of the total density of atoms or the atomic species partition function.

In our experiments, the transition lines at 13.178 nm (2p-5p), 14.705 nm (2s–4p), 19.253 nm (2p-3d), 20.240 nm (2p-3d), 22.742 nm (2p-3s), and 23.130 nm (2p-3d) for O V ions and some spectral lines of O IV ions were used, respectively, for the determination of the electron temperature, they are labeled in Figure 4 along with the calibrated lines and main carbon transitions. These lines are well resolved, the transition probabilities used here are provided by the NIST database [36] with a well-known uncertainty. The wavelengths, degeneracies, and transition probabilities of these oxygen lines are summarized in Table 1.

Boltzmann plots were constructed from the relative intensity of oxygen lines as shown in Figure 5. The experimental data were fitted by least-squares regression. The linear coefficient of regression r turned out to be $r > 0.9$ on average. As a result, the plasma temperature is 16.6 and 17.2 eV obtained from O V and O IV ions, respectively.

The validity of the local thermodynamic equilibrium assumption (LTE) was checked using McWhirter's criterion [43, 44], which requires the electron number density to satisfy the conditions: $N_e \geq 1.6 \times 10^{12} T^{1/2} (\Delta E)^3$, where $N_e\,(\mathrm{cm}^{-3})$ is the electron number density, $T(K)$ is the plasma temperature, and ΔE (eV) is the difference in the energies between the upper and lower states of all investigated transitions. With the evaluated temperature of 190 000 K in our experiment and $N_e = 4.1 \times 10^{20}\mathrm{cm}^{-3}$, the maximum energy gap ΔE at 14.705 nm, and the LTE requirements are met. The determination of the electron density will be discussed later in this section.

Furthermore, the plasma is optically thin for most lines, as checked from the absorption coefficient due to inverse Bremsstrahlung [45] and the effect of self-absorption [46]. In our experiment, the maximum absorption coefficient for inverse Bremsstrahlung is 0.057 cm^{-1} at 28.596 nm, since the plasma diameter is a millimeter, the weak absorption ($1/K_{\nu\max}$ = 17.5cm) due to inverse Bremsstrahlung does not affect our quantitative spectroscopy. For the optically thick lines of transitions to the ground state $1s^2 2p^2$, the intensities were modified according to the self-absorption coefficient.

For the uncertainty associated with the temperature obtained from the observed emission intensity, there are a number of factors that contribute to it. The main error of the Boltzmann-plot method arises from the uncertainty of the transition probability and the measurement error of the experimental spectral intensity. In our experiment, the transition probability accuracy of the spectral lines chosen for the evaluation is ≤10% [36], combined with the measured intensity error, the uncertainty caused by relative intensity, fitting, and transition probability is about 18%.

It should be noted that the temperature obtained by the Boltzmann-plot method is the time average temperature of the entire plasma [42]. The spatial distribution and temporal evolution of the plasma density and temperature at different times can be obtained by hydrodynamic simulations [18]. With a similar experimental design, the plasma temperature variation is estimated to be about 25% during the 5 to 20 ns time span. These uncertainties, however, do not cause directly similar uncertainty in the temperature determination. The relative uncertainty in the electron temperature determination by the Boltzmann-plot method scales with the factor T/E_m, which is the ratio of the thermal energy of the plasma T and the level energy E_m. As a result, we have estimated that our plasma temperature relative error is about 7%.

Also from previous experiments [18], it is well documented that foam layers show high hydrodynamic stability during the heating process. The matter density is almost constant and stays close to the initial line density value. As a

Table 1: Spectroscopic parameters of the observed oxygen lines for plasma temperature determination.

Wavelength (nm)			Transition				Intensity
Exp.	NIST	Ion	Configuration	Term	Degeneracies	A($\times 10^9$)	Exp.
13.871	13.8109	O V	$1s^2 2s2p$-$1s^2 2s5d$	$^3P_2$-$^3D_3$	5-7	11.2	0.072
14.705	14.7263	O V	$1s^2 2s2p$-$1s^2 2p4p$	$^1P_1$-$^1D_2$	3-5	9.52	0.036
19.253	19.2797	O V	$1s^2 2s2p$-$1s^2 2s3d$	$^3P_1$-$^3D_2$	3-5	51.7	0.796
20.240	20.2391	O V	$1s^2 2p^2$-$1s^2 2p3d$	$^3P_2$-$^3P_2$	5-5	34.3	0.202
22.742	22.7512	O V	$1s^2 2p^2$-$1s^2 2p3s$	$^3P_2$-$^3P_2$	5-5	10.3	0.105
23.151	23.1822	O V	$1s^2 2p^2$-$1s^2 2p3d$	$^1S_0$-$^1P_1$	1-3	43.6	0.137
23.356	23.3562	O IV	$2s2p^2$-$2s2p3d$	$^4P_{5/2}$-$^4D_{7/2}$	6-8	52.7	0.207
23.875	23.8570	O IV	$2s^2 2p$-$2s^2 3\,d$	$^2P_{3/2}$-$^2D_{5/2}$	4-6	35.4	0.241
25.299	25.3082	O IV	$2s2p^2$-$2s2p3d$	$^2P_{3/2}$-$^2D_{5/2}$	4-6	28.5	0.057
26.679	26.6931	O IV	$2s2p^2$-$2s2p3d$	$^2D_{5/2}$-$^2D_{5/2}$	6-6	14	0.049
28.596	28.5834	O IV	$2s2p^2$-$2s2p3d$	$^2S_{1/2}$-$^2P_{3/2}$	2-4	19.7	0.044

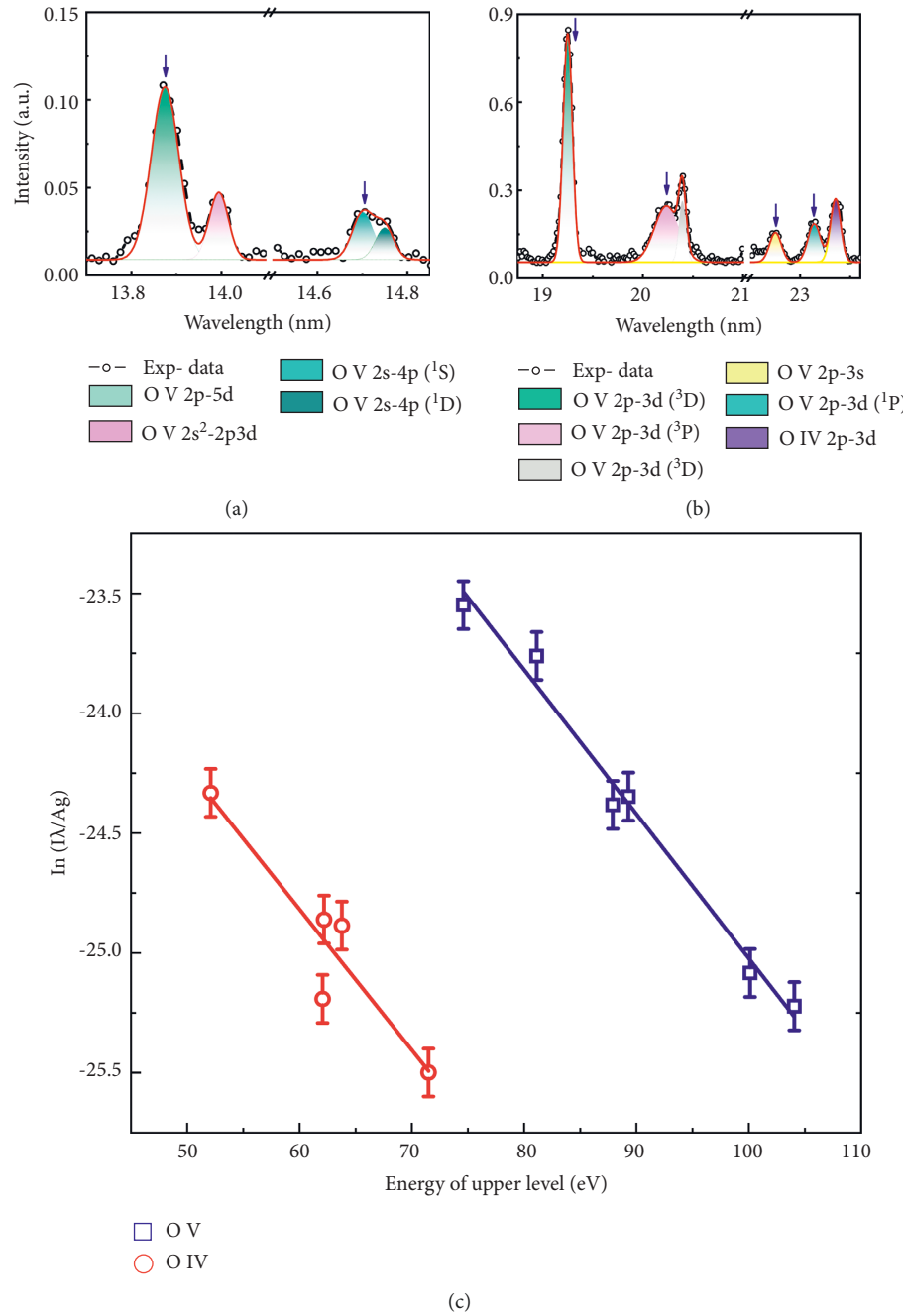

Figure 5: Results of plasma temperature. (a, b) The O V characteristic lines (arrows) that were used to construct the Boltzmann plot. Intensities were obtained by line fitting procedure with Gaussian line profiles, and the O IV lines can be treated similarly. (c) Boltzmann plots for O IV and O V emission lines.

result of this, the radiative heat wave is supersonic. Thus, the radiative heat transfer proceeds at a higher speed than the thermal expansion.

Calculation of the ion charge state distributions using the collisional radiative code FLYCHK [47] shows that the ionization degree of CHO foam is around $C_9^{3.80\pm0.03+}H_{16}^{0.98\pm0.003+}O_8^{4.33\pm0.2+}$ for the 16.8 ± 1.1 eV electron temperature that we obtained from the Boltzmann-plot method and the corresponding free electron density of $4.0 \pm 0.3 \times 10^{20}\text{cm}^{-3}$. Here the relative error is 7%. The mean ion charge state Z^{q+} is $q = 2$-3.

4. Conclusions

In our experimental campaign, we used a foam target (TCA) and subjected it to broadband thermal soft X-ray radiation generated in an attached cylindrical hohlraum. The resulting plasma is characterized by a large volume with high uniformity and long lifetime and near-critical density of free electrons of $4.0 \pm 0.3 \times 10^{20}\text{cm}^{-3}$ and a temperature of 16.8 ± 1.1 eV. We applied high-resolution spectroscopy to determine the hohlraum and plasma characteristics. We used a single-order diffraction grating and flat-field grating spectrometer. In addition, the spectroscopy and Boltzmann-plot method were successfully used for the diagnosis of plasma temperature by analyzing time-averaged emission spectra. The free electron density was determined based on the ionization degree and electronic structure information of the CHO plasma. Moreover, the plasma is a good test bed for laser-NCD (near-critical density) plasma interaction to generate high energy and brilliant charged particle and photon beams.

Data Availability

The data that support the findings of this study are available from the corresponding author upon reasonable request.

Conflicts of Interest

The authors declare that they have no conflicts of interest.

Authors' Contributions

Yongtao Zhao initiated and organized the experiments. Jieru Ren and Yongtao Zhao carried out the experiments together with the high-power laser team (Zongqing Zhao, Weimin Zhou, and Yuqiu Gu), the plasma diagnostics team, including the XRD team (Zhurong Cao, Xing Wang, Lirong Liu, and Bo Cui), the Flat Field Grating Spectrometer team (Shaoyi Wang, Bubo Ma, Yong Chen, and Leifeng Cao), the Transmission Grating Spectrometer team (Quanping Fan, Bubo Ma, Yong Chen, and Leifeng Cao) as well as the experimental setup installation and collimation team (Zhigang Deng, Wei Qi, Rui Cheng, Wenqing Wei, Xing Xu, Wei Liu, Shuai Yin, Jianhua Feng, Zhongmin Hu, and Hao Xu). Bubo Ma, Shaoyi Wang, Quanping Fan, and Jieru Ren analyzed the spectral data. Benzheng Chen, Shizheng Zhang, Zhongfeng Xu, Fangfang Li, Taotao Li, Yutian Li, Yingying Wang, Quanxi Xue, Yongtao Zhao, and Dieter Hoffmann contributed to the physical interpretation of experimental data. Bubo Ma, Jieru Ren, Yongtao Zhao, and Dieter Hoffmann drafted the article and all the coauthors revised the manuscript critically. Zhigang Deng, Wei Qi, Rui Cheng, Wenqing Wei, Xing Xu, Wei Liu, Shuai Yin, Jianhua Feng, Zhongmin Hu, Hao Xu, Zongqing Zhao, Weimin Zhou, and Yuqiu Gu made a critical revision to the experimental setup section and improved Figure 1. Zhurong Cao, Xing Wang, Lirong Liu, and Bo Cui made a critical revision in discussions related to Figure 2(a). Jieru Ren, Zhigang Deng, Wei Qi, and Wenqing Wei made critical modifications in discussions related to Figure 2(b). Quanping Fan, Bubo Ma, Yong Chen, and Leifeng Cao made a critical revision in discussions related to Figure 3. Shaoyi Wang, Yong Chen, and Leifeng Cao performed the design and calibration of the spectrometers and made a critical revision in discussions related to Figure 4. Benzheng Chen, Shizheng Zhang, Zhongfeng Xu, Fangfang Li, Taotao Li, Yutian Li, Yingying Wang, and Quanxi Xue made a critical revision in discussions related to the temperature determination. All the authors approved the final version to be published and agreed to be accountable for all aspects of the work in ensuring that questions related to the accuracy or integrity of any part of the work are appropriately investigated and resolved.

Acknowledgments

The experiment was performed at the XG-III facility in Mianyang. The authors are grateful to the staff of Laser Fusion Research Center. The work was supported by National Key R&D Program of China, No. 2019YFA0404900, Chinese Science Challenge Project, No. TZ2016005, National Natural Science Foundation of China (Grant Nos. U2030104, 12120101005, 12175174, and 11975174), China Postdoctoral Science Foundation (Grant no. 2017M623145), State Key Laboratory Foundation of Laser Interaction with Matter (Nos. SKLLIM1807 and SKLLIM2106), and the Fundamental Research Funds for the Central Universities.

References

[1] J. Nilsen, A. L. Kritcher, M. E. Martin et al., "Understanding the effects of radiative preheat and self-emission from shock heating on equation of state measurement at 100s of Mbar using spherically converging shock waves in a NIF hohlraum," *Matter and Radiation at Extremes*, vol. 5, no. 1, Article ID 018401, 2020.

[2] K. A. Tanaka, K. M. Spohr, D. L. Balabanski et al., "Current status and highlights of the ELI-NP research program," *Matter and Radiation at Extremes*, vol. 5, no. 2, Article ID 024402, 2020.

[3] F. Wang, S. E. Jiang, Y. K. Ding et al., "Recent diagnostic developments at the 100 kJ-level laser facility in China," *Matter and Radiation at Extremes*, vol. 5, no. 3, Article ID 035201, 2020.

[4] B. Y. Sharkov, D. H. H. Hoffmann, A. A. Golubev, and Y. T. Zhao, "High energy density physics with intense ion beams," *Matter and Radiation at Extremes*, vol. 1, no. 1, pp. 28–47, 2016.

[5] X. Y. Zhao, Y. Y. Yang, H. Jia et al., "Influence of the solenoid magnetic field on the self-modulation mechanism," *Laser and Particle Beams*, vol. 38, no. 2, pp. 135–140, 2020.

[6] D. Böhne, I. Hofmann, G. Kessler et al., "HIBALL—a conceptual design study of a heavy-ion driven inertial confinement fusion power plant," *Nuclear Engineering and Design*, vol. 73, no. 2, pp. 195–200, 1982.

[7] I. Hofmann, "HIDIF–an approach to high repetition rate inertial fusion with heavy ions," *Nuclear Instruments and Methods in Physics Research Section A: Accelerators, Spectrometers, Detectors and Associated Equipment*, vol. 415, no. 1-2, pp. 11–19, 1998.

[8] J. Hornung, Y. Zobus, S. Roeder et al., "Time-resolved study of holeboring in realistic experimental conditions," *Nature Communications*, vol. 12, no. 1, p. 6999, 2021.

[9] D. Dojic, M. Skocic, and S. Bukvic, "Shielding effects in interaction of nanosecond laser pulses with solid target," *Spectrochimica Acta Part B: Atomic Spectroscopy*, vol. 186, Article ID 106319, 2021.

[10] T. A. Meinhold and N. Kumar, "Radiation pressure acceleration of protons from structured thin-foil targets," *Journal of Plasma Physics*, vol. 87, no. 6, Article ID 905870607, 2021.

[11] A. Frank, A. Blazevic, P. L. Grande et al., "Energy loss of argon in a laser-generated carbon plasma," *Physical Review E*, vol. 81, no. 2, Article ID 026401, 2010.

[12] A. Frank, A. Blazevic, V. Bagnoud et al., "Energy loss and charge transfer of argon in a laser-generated carbon plasma," *Physical Review Letters*, vol. 110, no. 11, Article ID 115001, 2013.

[13] W. Cayzac, A. Frank, A. Ortner et al., "Experimental discrimination of ion stopping models near the Bragg peak in highly ionized matter," *Nature Communications*, vol. 8, no. 1, Article ID 15693, 2017.

[14] P. Neumayer, R. Bock, S. Borneis et al., "Status of PHELIX laser and first experiments," *Laser and Particle Beams*, vol. 23, no. 3, pp. 385–389, 2005.

[15] G. Schaumann, M. S. Schollmeier, G. Rodriguez-Prieto et al., "High energy heavy ion jets emerging from laser plasma generated by long pulse laser beams from the NHELIX laser system at GSI," *Laser and Particle Beams*, vol. 23, no. 4, pp. 503–512, 2005.

[16] O. N. Rosmej, V. Bagnoud, U. Eisenbarth et al., "Heating of low-density CHO-foam layers by means of soft *X*-rays," *Nuclear Instruments and Methods in Physics Research Section A: Accelerators, Spectrometers, Detectors and Associated Equipment*, vol. 653, no. 1, pp. 52–57, 2011.

[17] S. Faik, A. Tauschwitz, M. M. Basko et al., "Creation of a homogeneous plasma column by means of hohlraum radiation for ion-stopping measurements," *High Energy Density Physics*, vol. 10, no. 3, pp. 47–55, 2014.

[18] O. N. Rosmej, N. Suslov, D. Martsovenko et al., "The hydrodynamic and radiative properties of low-density foams heated by *X*-rays," *Plasma Physics and Controlled Fusion*, vol. 57, no. 9, Article ID 094001, 2015.

[19] G. Belyaev, M. Basko, A. Cherkasov et al., "Measurement of the Coulomb energy loss by fast protons in a plasma target," *Physical Review E*, vol. 53, no. 3, pp. 2701–2707, 1996.

[20] D. H. H. Hoffmann, V. E. Fortov, I. V. Lomonosov et al., "Unique capabilities of an intense heavy ion beam as a tool for equation-of-state studies," *Physics of Plasmas*, vol. 9, no. 9, pp. 3651–3654, 2002.

[21] E. Nardi, Y. Maron, and D. H. H. Hoffmann, "Plasma diagnostics by means of the scattering of electrons and proton beams," *Laser and Particle Beams*, vol. 25, no. 3, pp. 489–495, 2007.

[22] G. Xu, M. D. Barriga-Carrasco, A. Blazevic et al., "Determination of hydrogen density by swift heavy ions," *Physical Review Letters*, vol. 119, no. 20, Article ID 204801, 2017.

[23] J. R. Ren, Z. G. Deng, W. Qi et al., "Observation of a high degree of stopping for laser-accelerated intense proton beams in dense ionized matter," *Nature Communications*, vol. 11, no. 1, p. 5157, 2020.

[24] A. J. Mackinnon, P. K. Patel, R. P. Town et al., "Proton radiography as an electromagnetic field and density perturbation diagnostic (invited)," *Review of Scientific Instruments*, vol. 75, no. 10, pp. 3531–3536, 2004.

[25] G. Sarri, A. Macchi, C. A. Cecchetti et al., "Dynamics of self-generated, large amplitude magnetic fields following high-intensity laser matter interaction," *Physical Review Letters*, vol. 109, no. 20, Article ID 205002, 2012.

[26] B. B. Ma, J. R. Ren, S. Y. Wang et al., "Laboratory observation of C and O emission lines of the white dwarf H1504+65-like atmosphere model," *The Astrophysical Journal*, vol. 920, no. 2, p. 106, 2021.

[27] J. Q. Su, Q. H. Zhu, N. Xie et al., "Progress on the XG-III high-intensity laser facility with three synchronized beams," *Proceedings of SPIE*, vol. 9255, Article ID 925511, 2015.

[28] L. Wei, Y. Chen, S. Wang et al., "Suppression of higher diffraction orders using quasiperiodic array of rectangular holes with large size tolerance," *High Power Laser and Particle Beams*, vol. 32, no. 7, pp. 1001–4322, 2020.

[29] Y. W. Liu, X. L. Zhu, Y. L. Gao et al., "Quasi suppression of higher-order diffractions with inclined rectangular apertures gratings," *Scientific Reports*, vol. 5, no. 1, Article ID 16502, 2015.

[30] A. L. Meadowcroft, C. D. Bentley, and E. N. Stott, "Evaluation of the sensitivity and fading characteristics of an image plate system for x-ray diagnostics," *Review of Scientific Instruments*, vol. 79, no. 11, Article ID 113102, 2008.

[31] Y. T. Zhao, Y. N. Zhang, R. Cheng et al., "Benchmark experiment to prove the role of projectile excited states upon the ion stopping in plasmas," *Physical Review Letters*, vol. 126, no. 11, Article ID 115001, 2021.

[32] O. Ciricosta, S. M. Vinko, H. K. Chung et al., "Direct measurements of the ionization potential depression in a dense plasma," *Physical Review Letters*, vol. 109, no. 6, Article ID 065002, 2012.

[33] G. Del Zanna, K. P. Dere, P. R. Young, and E. Landi, "Chianti-an atomic database for emission lines. XVI. Version 10, further extensions," *The Astrophysical Journal*, vol. 909, no. 1, p. 38, 2021.

[34] E. Landi and P. R. Young, "Chianti-An Atomic Database for Emission Lines. X. spectral atlas of a cold feature observed with HINODE/EUV imaging spectrometer," *The Astrophysical Journal*, vol. 706, no. 1, pp. 1–20, 2009.

[35] E. Träbert, P. Beiersdorfer, N. S. Brickhouse, and L. Golub, "Low-density laboratory spectra near the He II lambda 304 line," *Astronomy & Astrophysics*, vol. 586, p. A115, 2016.

[36] A. Kramida, Y. Ralchenko, and J. Reader, "NIST atomic spectroscopic databases," 2020, https://physics.nist.gov/asd.

[37] B. Zhongmou, "Hefei national Synchrotron radiation laboratory," *Physica Scripta*, vol. 36, no. 1, pp. 65–68, 1987.

[38] L. Wei-Min, W. Lin, F. Guang-Yao et al., "Conceptual design of Hefei advanced light source," *Chinese Physics C*, vol. 33, no. S2, pp. 128–130, 2009.

[39] X. W. Du, Y. C. Shen, C. Y. Li, N. An, Y. Shi, and Qp Wang, "EUV flat field grating spectrometer and performance

measurement," *Spectroscopy and Spectral Analysis*, vol. 32, no. 8, pp. 2270–2274, 2012.

[40] F. Lu, G. Li, X. L. Wen et al., "Calibration of sensitivity function for image plate scanner," *Atomic Energy Science and Technology*, vol. 52, no. 3, pp. 528–532, 2018.

[41] G. J. Williams, B. R. Maddox, H. Chen, S. Kojima, and M. Millecchia, "Calibration and equivalency analysis of image plate scanners," *Review of Scientific Instruments*, vol. 85, no. 11, Article ID 11E604, 2014.

[42] N. M. Shaikh, S. Hafeez, B. Rashid, S. Mahmood, and M. A. Baig, "Optical emission studies of the mercury plasma generated by the fundamental, second and third harmonics of a Nd: YAG laser," *Journal of Physics D: Applied Physics*, vol. 39, no. 20, pp. 4377–4385, 2006.

[43] L. J. Martino and C. A. D'Angelo, "Diagnostics of laser induced plasmas at late delay times," *Journal of Analytical Atomic Spectrometry*, vol. 35, no. 5, pp. 1003–1010, 2020.

[44] E. Mal, R. Junjuri, M. K. Gundawar, and A. Khare, "Temporal characterization of laser-induced plasma of tungsten in air," *Laser and Particle Beams*, vol. 38, no. 1, pp. 14–24, 2020.

[45] J. T. Knudtson, W. B. Green, and D. G. Sutton, "The UV-visible spectroscopy of laser-produced aluminum plasmas," *Journal of Applied Physics*, vol. 61, no. 10, pp. 4771–4780, 1987.

[46] N. M. Shaikh, B. Rashid, S. Hafeez, Y. Jamil, and M. A. Baig, "Measurement of electron density and temperature of a laser-induced Zinc plasma," *Journal of Physics D: Applied Physics*, vol. 39, no. 7, pp. 1384–1391, 2006.

[47] R. W. Lee, M. H. Chen, W. L. Morgan, and H.-K. Chung, "FLYCHK: a straightforward, general population kinetics and spectrum modeling capability," in *Proceedings of the IEEE Conference Record - Abstracts. 2005 IEEE International Conference on Plasma Science - ICOPS 2005*, p. 94, Monterey, CA, USA, June 2005.